Quaternary Science Reviews 346 (2024) 109070

Contents lists available at ScienceDirect

Quaternary Science Reviews

journal homepage: www.elsevier.com/locate/quascirev

Reconstructing Holocene hydroclimate variability and coastal dynamics of the Nile Delta: A diatom perspective

Yanna Wang [a], Jinqing Zhou [b], Xiaoshuang Zhao [a,*], David Kaniewski [c], Nick Marriner [d], Alaa Salem [e], Jing Chen [a], Zhongyuan Chen [a]

[a] The State Key Laboratory of Estuarine and Coastal Research, East China Normal University, Shanghai, 200062, China
[b] School of Geography and Ocean Science, Nanjing University, Nanjing, 210023, Jiangsu, China
[c] Centre de Recherche sur la Biodiversité et l'Environnement (CRBE), Université de Toulouse, CNRS, IRD, Toulouse INP, Université Toulouse 3 - Paul Sabatier (UT3), Toulouse, France
[d] CNRS, ThéMA, Université de Franche-Comté, UMR 6049, MSHE Ledoux, 32 rue Mégevand, 25030, Besançon, Cedex, France
[e] Faculty of Science, Kafrelsheikh University, Kafrelsheikh, Egypt

ARTICLE INFO

Handling editor: I Hendy

Keywords:
Palaeo-Nile flow
Aulacoseira granulata
Delta-coast habitat
Sea-level rise
Holocene
African Humid Period

ABSTRACT

This study analyses diatom assemblages from a Nile Delta core (B-1) to probe Holocene hydroclimate changesand their influence on the ecological habitats of the delta coast, with a further focus on the effects of relative sea-level rise. We found that the freshwater diatom *Aulacoseira granulata* varied in tandem with hydroclimate pulses in the Nile watershed, driven by the shift of the Intertropical Convergence Zone (ITCZ), therefore serving as a proxy for palaeo-Nile flow. Based on the ecological affinities of diatom taxa, we defined 5 diatom assemblages (I-V). Assemblage I (>10.0-8.5 ka BP) shows high *A. granulata* abundance (60–80%), implying peak Nile flow during the African Humid Period (AHP), at least 3 times greater than that of the recent past. Assemblage II (8.5-7.5 ka BP) sees decreased *A. granulata* (20–40%) and emergence of freshwater diatoms with benthic-oligotrophic characteristics (e.g. *Epithemia gibba*), suggesting reduced Nile flow and a delta estuary where the habitat became shallower with lower nutrient content. Assemblage III (7.5-6.0 ka BP) shows *A. granulata* resurgence (50–80%), reflecting Nile hydroclimate variability post-AHP due to the migration of the Intertropical Convergence Zone (ITCZ). The high-resolution- diatom spectra of B-1 also revealed major habitat changes, from saline to fluvial-dominated environments, around 6.0 ka BP. Assemblage IV (6.0-3.2 ka BP) indicates a notable Nile flow decline and freshwater community proliferation, coinciding with coastal habitat expansion and delta progradation due to RSL stablisation and basin-wide aridification. Assemblage V (3.2-2.0 ka BP) is marked by drought-tolerant diatoms (*Nitzchia amphibia, Hantzschia amphioxys* and *Cavinula cocconeiformis*), indicating intensified aridification.

1. Introduction

In the context of investigating human occupation and basin-wide hydroclimate changes due to relative sea-level rise, the Nile Delta and its associated sediment archives are of significant scientific interest (Fig. 1). During the Holocene, the region is characterised by not only the arid climatic conditions prevalent in the lower basin but also by significant hydrodynamic changes observed in the upper basin, particularly in the context of interactions between the Indian monsoon, the African monsoon and the Congo Air Boundary (CAB) (Butzer, 1976; Said, 1981). Huge amounts of water and sediment have been washed downstream to feed the delta coast, mainly from the African Highlands and the Ethiopian Plateau where heavy rainfall attained ca. 1400–2000 mm per year (Vizy and Cook, 2003; Slingo et al., 2005; Wolman and Giegengack, 2007).

In the early Holocene, the northward migration of the Intertropical Convergence Zone (ITCZ) caused a prolonged humid period over North Africa, known as the African Humid Period (AHP, generally, ca. 14.5–5.0 ka BP) (Woodward et al., 2007; Macklin et al., 2012; Shanahan et al., 2015; Tierney et al., 2017; Pausata et al., 2020). During this period, the monsoon rain belt expanded northwards turning the Sahara into the 'Green Sahara' and creating conditions that supported early

* Corresponding author. The State Key Laboratory of Estuarine and Coastal Research, East China Normal University, Shanghai, 200062, China.
E-mail address: xszhao@sklec.ecnu.edu.cn (X. Zhao).

https://doi.org/10.1016/j.quascirev.2024.109070
Received 3 May 2024; Received in revised form 2 October 2024; Accepted 7 November 2024
Available online 19 November 2024

agricultural development (Tierney et al., 2017). Strong Nile flow transported huge quantities of alluvium to shape the sedimentary-ecological environments of the Early-Holocene Nile estuary before the delta had formed (Stanley and Warne, 1993a; Giaime et al., 2022; Wang et al., 2022). The tropical hydroclimate of eastern Africa became unstable as the ITCZ retreated around 7.5-4.5 ka BP, driven by precession-forced equatorial insolation (Rossignol-Strick, 1983). Accordingly, the meridional movement of eastern Africa hydroclimate exerted a greater hydro-forcing role on the formation of the delta-estuary environment (Wang et al., 2022).

The delta eco-setting was also influenced by Holocene sea-level rise (Stanley and Warne, 1993a), characterised by high relative sea-level rising rates before ca. 8.0-7.0 ka BP and then followed by a pronounced deceleration until ca. 4.0-2.0 ka BP (Arbouille and Stanley, 1991; Stanley and Warne, 1993b; Giaime et al., 2022). Given the significant differences in relative sea-level rise across different sectors of the Nile Delta (Stanley and Clemente, 2017), the processes by which the former saline estuarine habitat of the north-central Nile coast evolved into a fluvial environment—through prolonged interaction between Nile flow and marine incursions remains unclear.

Formed under the dual hydro-forcings of watershed and marine dynamics, the lagoon areas of the Nile Delta have received a continuous supply of sediment, yielding archives to track Holocene changes in palaeo-hydroclimate and coastal habitats (Marriner et al., 2013). In the past, many studies have effectively reconstructed Holocene environmental change by using multiple bio-geochemical proxies of the lagoon sediments (e. g. Arbouille and Stanley, 1991; Krom et al., 2002; Bernhardt et al., 2012; Giaime et al., 2022; Zhang et al., 2022). By analysing biogenic and non-biogenic elements (C, N, P and Si), isotope ($\delta^{13}C$, $\delta^{15}N$ and $\delta^{18}O$) and biomarkers (Chlorophyll, sterols and n-alkanes) of the lagoonal sediments, palaeo-hydroclimate and marine impacts have been elucidated. However, key knowledge gaps remain relating to the temporal and spatial scales of Holocene changes. For instance, the termination of the AHP and the impact of palaeo-hydroclimate change on Nile flow variations are topics of ongoing scientific debate (deMenocal et al., 2000; Tierney et al., 2010; Marshall et al., 2011).

With a wide ecological range from freshwater to marine aquatic habitats, diatoms are a robust biological proxy to explore paleoenvironmental change (Smol and Stoermer, 2010). In particular, diagnostic diatom communities preserved in lagoon sediments can provide high-resolution data to not only probe hydroclimate fluctuations but also investigate the role of delta-coast changes and eco-setting. Using the distinctive salinity-tolerance of diatom taxa, terrestrial and marine influences can be reconstructed to help better understand the processes and consequences of environmental changes, leading to insightful perspectives for future studies (e. g. Uścinowicz et al., 2007; Carvalho do Amaral et al., 2012; Winsborough et al., 2012; Schallenberg and Saulnier-Talbot, 2014; Koutsodendris et al., 2017; Nakanishi et al., 2017).

Of note, there have been extensive studies conducted on tracking hydroclimate change in the upper Nile basin area (the African Great Lake region) and the eastern Mediterranean Sea (Emeis et al., 2000, 2003; Box et al., 2011). Strong hydroclimate correlations between these two regions have been observed at various spatiotemporal scales (Castañeda et al., 2016). The present study looks to bridge knowledge across the two regions, using sensitive diatom proxies to investigate: 1) diatom-specific implications in the reconstruction of the palaeo-hydroclimate changes; 2) the role of palaeo-Nile flow in the development of delta-estuarine habitats; and 3) basin-scale hydroclimate forcing agents. To fill these knowledge gaps, we chose the continuous core B-1 retrieved from Burullus lagoon on the central Nile Delta.

2. Materials and methods

2.1. Sediment coring, logging and sampling

A sediment core, B-1, measuring 8.7 m in length and situated 3.0 m above mean sea level (msl), was drilled on the coastal plain, 40 km south of the Burullus lagoon coast (31°11′58″N, 30°44′26″E) (Figs. 1 and 2). To avoid potential biases in diatom preservation and identification associated with the delta coast, the core site was strategically located on the inner lagoon coast, where conditions favour continuous sedimentation and provide a suitable Holocene sediment thickness for scientific study (Figs. 1 and 2). This site selection was further informed by insights from our previous core BR-1 on the open coast of study area (Fig. 1), where

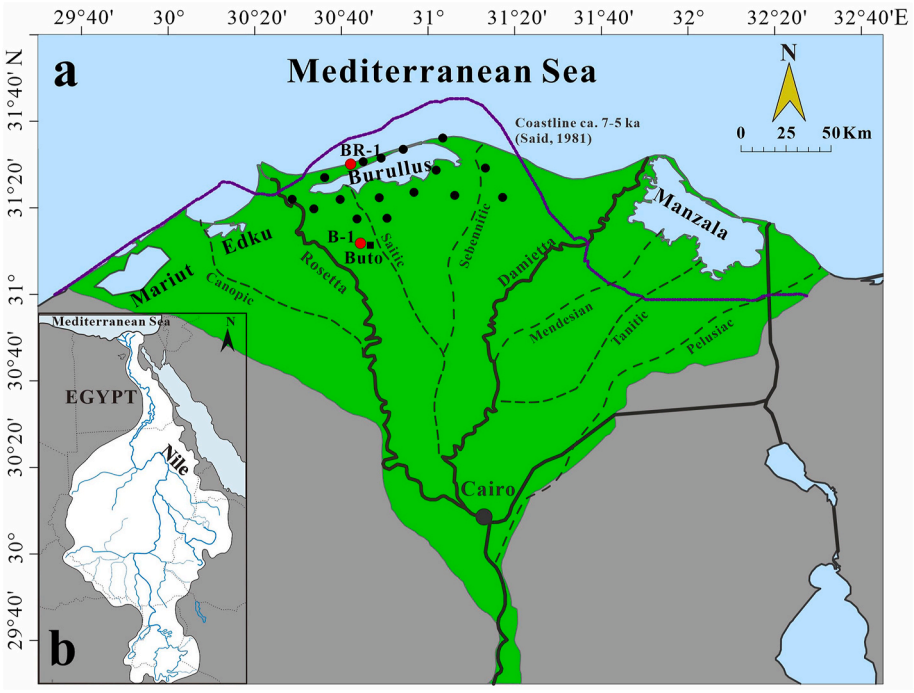

Fig. 1. The Nile Delta area, showing a) the location of sediment core B-1, and the sediment cores collected in previous studies; and b) the Nile River basin.

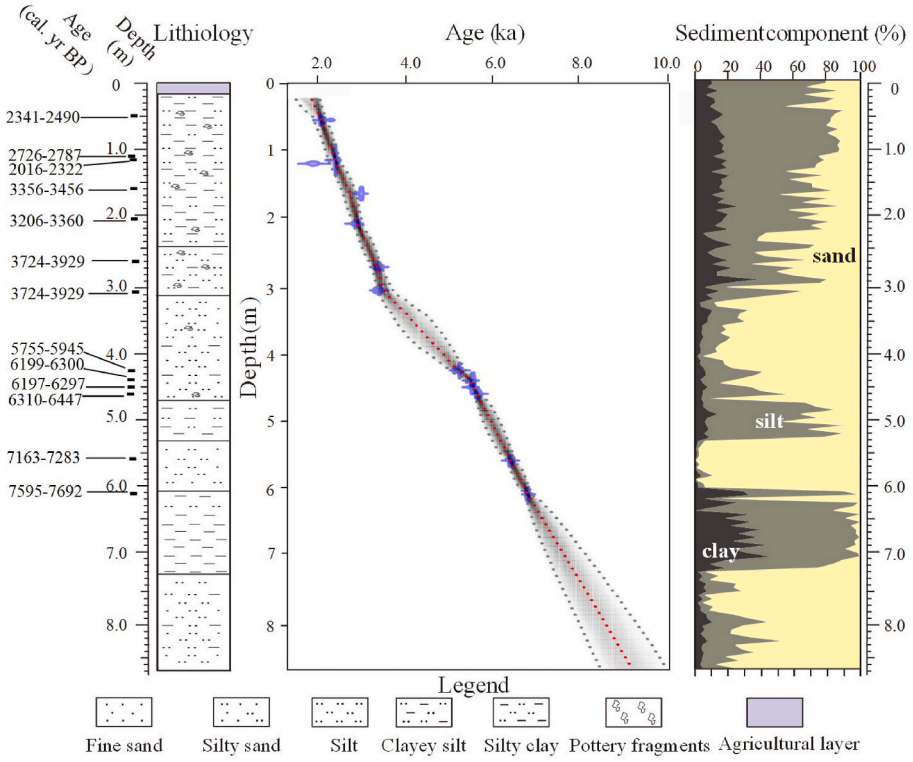

Fig. 2. AMS ^{14}C-dated Holocene strata of core B-1 and associated sediment texture. The age model is based on 13 dates.

high sedimentation rates during the Holocene have been documented (Giaime et al., 2022).

Core samples were collected continuously using a COBRA vibra-corer equipped with 2.0-m long tubes with a diameter of 9.0 cm. Core samples were stored in wooden boxes and transported to the laboratory for further analysis. The core was split into two halves, one for logging and the other for archiving. Core sediment was described including sediment colour, water content, lithology and biogenesis. Core sediment was then sampled at regular 5-cm intervals and dried via lyophilisation before analysis. A thin agricultural layer (0–40 cm; Fig. 2) at the top of the core was not considered for diatom analysis to avoid impacts from recent human activities. Also, we reasoned that the linearly-dated Holocene sediments of B-1 (Fig. 2) provide a reliabile decadal-to-centennial-scale record of diatom communities, even though the influence of taphonomic processes along the delta coast cannot be entirely excluded (Espinosa et al., 2022).

2.2. Radiocarbon dating, age-depth model, and Holocene sea-level reconstruction

In total, thirteen sediment samples (12 organic muds and one shell fragment) from B-1 were sent to Beta Analytic in Florida, USA for AMS dating (Table 1). The ^{14}C dates were calibrated into calendar years before present (cal. yr BP) at confidence intervals of 95.4% (2σ), using the "rBacon" package for (Blaauw and Christen, 2011) and the IntCal 20 curve and Marine 20 curve (Blaauw and Christen, 2011; Heaton et al., 2020; Reimer et al., 2020) and a marine reservoir age of $\triangle R = 400 \pm 79$ yr. Age-depth calculations for all dates, expressed as "ka BP", were performed using the method described by Blaauw and Christen (2011). The Holocene sea-level curve of the study area was reconstructed using 20 dated lagoon-peats, including 3 from B-1, 4 from BR-1 (Fig. 3a) (Giaime et al., 2022) and 13 from Arbouille and Stanley (1991). The topographic elevation of the core sites was benchmarked relative to msl (see Giaime et al., 2022 for detailed methodology). We utilised the Errors-In-Variables Integrated Gaussian Process (EIV-IGP) model (Cahill et al., 2016) to calculate rates of Relative Sea Level (RSL) change from

Table 1
Radiocarbon dates of core B-1.

Core name	Depth (m)	Laboratory No.	Materials	Conventional age (yr BP)	Calibrated age (cal. yr BP)	d^{13}C (‰)
B-1	0.50	Beta-571272	Organic mud sediment	2380 ± 30 BP	2341–2490	−21.7
B-1	1.10	Beta-571274	Organic mud sediment	2360 ± 30 BP	2726–2787	−21.9
B-1	1.15	Beta-600306	Shell fragment	2650 ± 30 BP	2016–2322	−11.9
B-1	1.60	Beta-560433	Organic mud sediment	3180 ± 30 BP	3356–3456	−18.5
B-1	2.05	Beta-571275	Organic mud sediment	3060 ± 30 BP	3206–3360	−21.3
B-1	2.70	Beta-560434	Organic mud sediment	3560 ± 30 BP	3724–3929	−19.2
B-1	3.05	Beta-571276	Organic mud sediment	3560 ± 30 BP	3724–3929	−17.8
B-1	4.25	Beta-560435	Organic mud sediment	5140 ± 30 BP	5755–5945	−22.6
B-1	4.40	Beta-600306	Organic mud sediment	*5450 ± 30 BP*	6199–6300	−17.0
B-1	4.50	Beta-600307	Organic mud sediment	*5440 ± 30 BP*	6197–6297	−18.4
B-1	4.60	Beta-571277	Organic mud sediment	5610 ± 30 BP	6310–6447	−19.7
B-1	5.60	Beta-600986	Organic mud sediment	6310 ± 30 BP	7163–7283	−20.4
B-1	6.10	Beta-548856	Organic mud sediment	6820 ± 30 BP	7595–7692	−16.4

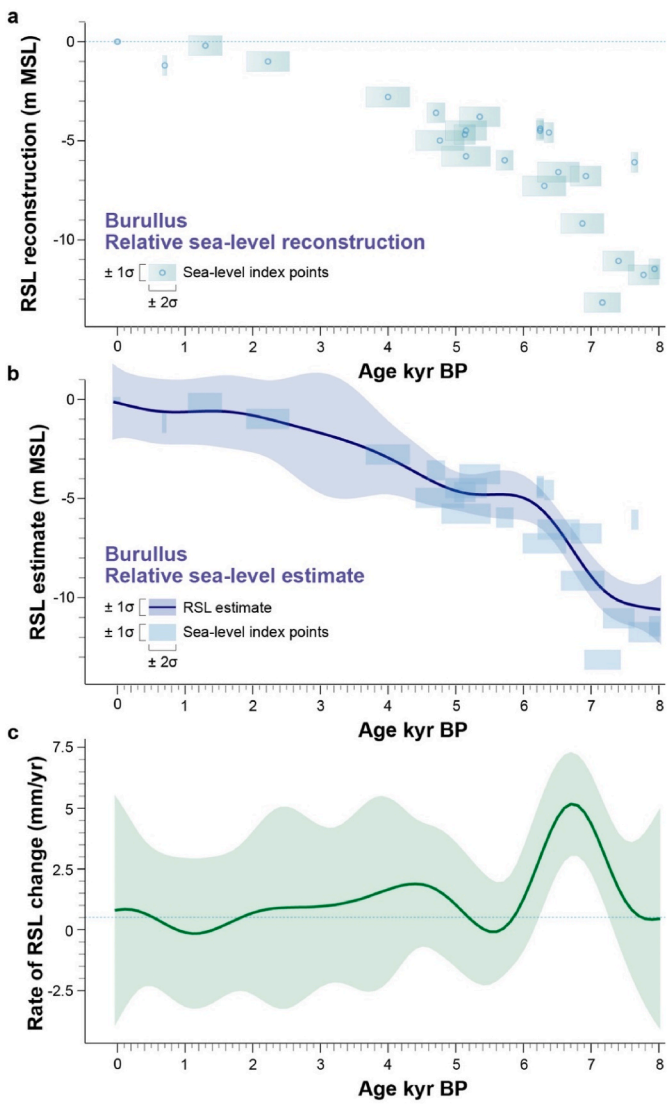

Fig. 3. Standardised RSL reconstruction for the Buto coast from 8000 ka BP to present. a) The RSL history is based on 20 SLIPS. The blue boxes represent the SLIPS from the lagoons and salt marshes. The dimensions of the boxes denote the ± 1σ altitudinal and ± 2σ chronological errors associated with each SLIP. b) Errors-In-Variables Integrated Gaussian Process model (EIV-IGP; Cahill et al., 2016) for RSL estimates (with the 1σ altitudinal error). c) Holocene RSL rising rates denoted in mm/yr.

Sea-Level Index Points (SLIPs) (Fig. 3b), applying a local Glacial Isostatic Adjustment (GIA) correction of -0.0512 mm^{-1} (Marriner et al., 2023). The EIV-IGP model employs a Gaussian Process prior on RSL rate estimates and integrates this process to derive estimations of the underlying RSL trend (Cahill et al., 2016). To tackle temporal uncertainty, this method is nested within an Errors-In-Variables framework. RSL uncertainties associated with the SLIPs are accommodated within the statistical model by introducing observation-specific error terms in the RSL data model. This modeling strategy offers a comprehensive assessment of uncertainty in both RSL estimates (Fig. 3) and the inferred rates of RSL change over time (Cahill et al., 2016).

2.3. Grain size

A total of 154 sediment samples was taken from B-1 for grain size analysis using ultrasonic methods (S_Table 1). Approximately 0.1-g of pre-homogenized sediment was pretreated with a 30% H_2O_2 solution to oxidize organic matter and a 10% HCl solution to remove carbonates. Before analysis, all of the sample was dispersed and homogenized using a solution of sodium hexametaphosphate. Grain size was measured using a Beckman Coulter LS13 320 Particle Size Analyzer.

2.4. Diatom analysis

Diatom fossil analysis was performed on 54 samples from B-1, selected at sampling intervals of 5–20 cm. Samples with few frustules were not taken into account (S_Table 1). Diatom frustules were isolated using the flotation method and identified following the procedures outlined in Renberg (1990) and Battarbee et al. (2001). Diatom taxa were identified and counted under a microscope at magnifications of 400 × and 1000 × .

In B-1, siliceous microfossils appeared well preserved: several fragile taxa including *Nitzschia* spp., *Tryblionella* spp. and *Pinnularia* spp. could be identified to species level with relatively intact frustules. *Aulacoseira granulata* could often be seen in chains with over two cells. In order to further verify the efficiency of diatom preservation in B-1, five random slides were examined to estimate the ratio of intact frustules at 400 × according to the method of McQuoid and Hobson (2001). The ratios of intact frustules on all the five slides were calculated to be over 60%.

Given the relatively constant sedimentation rates for core B-1, the absolute abundance (D_{abs}, valves/g DW) of diatom frustules can reflect the changes in diatom assemblages throughout the core sample. The relative abundance of each taxon (D_{re}, %) was calculated as a percentage (%) based on the total number of valves in each sample. Planktonic and benthic taxa were separately summed to show their temporal change along with other proxies.

Following Muylaert et al. (2009) and Baselga (2010), alpha diversity (D_α) and beta diversity (β_{sim}) were also computed to further determine the gradual compositional turnovers of assemblages in chronological order.

$$D_\alpha = 1 - \sum {D_{re}}^2 \quad (1)$$

$$\beta_{sim} = \frac{\min(b,c)}{a + \min(b,c)} \quad (2)$$

In the context of two adjacent samples, the variables a, b and c denote, respectively, the abundance of shared species, the abundance of species exclusive to one sample, and the abundance of species exclusive to the other.

Multiple statistical methods were applied to identify significant ecological changes in the diatom assemblages. Before testing, only taxa with a relative abundance of ≥0.5% and appearing in no less than 3 samples were selected for the analysis. This was mainly to avoid the influence of rare species on the significance tests (Katoh, 1993). D_{re} matrix data of diatoms were firstly run for their ecological affinity using the two-way indicator species analysis (TWINSPAN) in WinTWINS Version 2.3 (Hill and Šmilauer, 2005), which helps classify different taxa groups according to their similarities. From this base, the diatom dataset was further analysed by CONISS using the software Tilia (Grimm, 1987) to establish a chrono-ecological zonation of B-1. The principal component analysis (PCA) in the CANOCO Version 4.5 (ter Braak and Smilauer, 2002) was also applied to distinguish the typical species and potential controlling factors. In CANOCO, to further determine the waxing and waning of taxa in various time periods, the variations of taxa in chronological order were modeled using general additive modelling-GAM (Hastie and Tibshirani, 1990). Stepwise selection using the Akaike information criterion applied to the complexity control of the GAM model (Hastie and Tibshirani, 1990), and the maximum number of degrees of freedom for the smoother term was set to 2.

Sediment core BR-1 from our previous study, and further cores from the study area, were incorporated into our sedimentological database (Fig. 1) (Arbouille and Stanley, 1991; Giaime et al., 2021).

3. Results

3.1. Holoc\ene strata and relative sea-level curve

Sediment core B-1 revealed a series of Holocene strata typical of lagoonal-coastal environments in the central Nile Delta (Fig. 2) (Stanley et al., 1996). The dark grayish lagoonal muds, rich in organic matter occurred in the Holocene sediments. The yellowish sand sections with brackish shell fragments and diatoms prevailed in the lower-middle part (below core depth of 3.8 m) of the sediment core, which was interlayered with lagoonal muds (Fig. 2). Silt and clay with brackish-freshwater shell fragments and diatoms gradually became predominant (>50%) in the upper core sediment (Fig. 2). A thin agricultural soil (0.15–0 m) occurred on the core top. The age-depth model revealed the full Holocene strata of B-1, corresponding to the core's bottom at 8.7 m depth (Fig. 2). Based on the age model, relatively stable sedimentation rates were observed, ranging between 0.6 and 1.2 mm/year (Fig. 2).

The reconstructed Holocene relative sea-level curve of the study area showed that RSL was 12.0 m below msl ca. 8.0 ka BP. RSL rose rapidly between 8.0 ka and 6.0 ka BP, before plateauing at around 4 m below MSL between 6.0 ka and 5.0 ka BP. RSL then gradually rose over the next 5000 years, reaching present levels (Fig. 3). The interaction between sea-level rise and paleo-Nile flow will be explored in the following sections, describing their collective impact on the ecological habitat of the Nile Delta.

3.2. Ecological affinity

A total of 27 taxa was used for multiple statistical analyses after removing the rare species (S_Table 1). TWINSPAN was firstly applied with 9 levels (0, 1%, 2%, 5%, 10%, 15%, 20%, 40%, 60%) to classify taxa into 5 groups (Groups 1–5) according to their similarities (Fig. 4). These groups were differentiated on the basis of marine to fluvial habitats, to support the temporal zonation in CONISS (Fig. 5). Group 1 included mostly marine and brackish taxa. Group 2 consists primarily of brackish to freshwater taxa. Group 3 was dominated by freshwater taxa, and Groups 4 and 5 included freshwater and drought-tolerant species. It is worth noting that some species in Group 1 (including *Staurosira construens*, *Stephanodiscus hantzschii*, and *Campylodiscus clypeus*) and Groups 4 and 5 (including *Staurosira venter*, *Nitzschia umbonata*, *Surirella ovalis*, and *Nitzschia vitrea*) (Fig. 4) are referred to as marine-freshwater species because they have been found to live in both freshwater and seawater (https://www.algaebase.org/). In the present study, we attributed species in Group 1 to the marine domain and those in Groups 4–5 as having freshwater-brackish affinities based on the similarities to their contiguous taxa (Fig. 4).

3.3. Holocene diatom assemblages

Based on the characteristics of diatom assemblages identified in the CONISS analysis, there were 5 Holocene diatom assemblages (I-V) established in chronological order (older to younger) in B-1. Three subunits (A-C) were assigned to assemblage IV (Fig. 5).

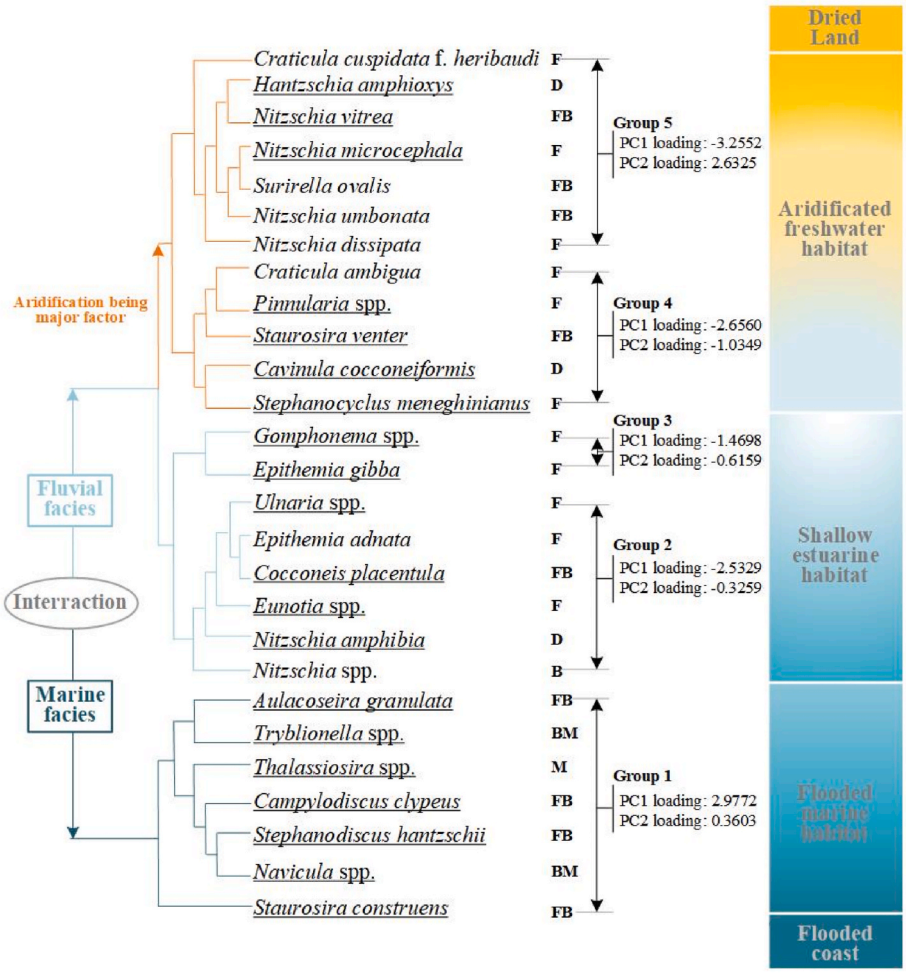

Fig. 4. Ecological affinities of diatom taxa from core B-1, based on TWINSPAN analysis. F-freshwater taxa; D-drought tolerant species; FB- freshwater-brackish species; B-brackish taxa; BM-brackish and marine taxa; M-marine taxa.

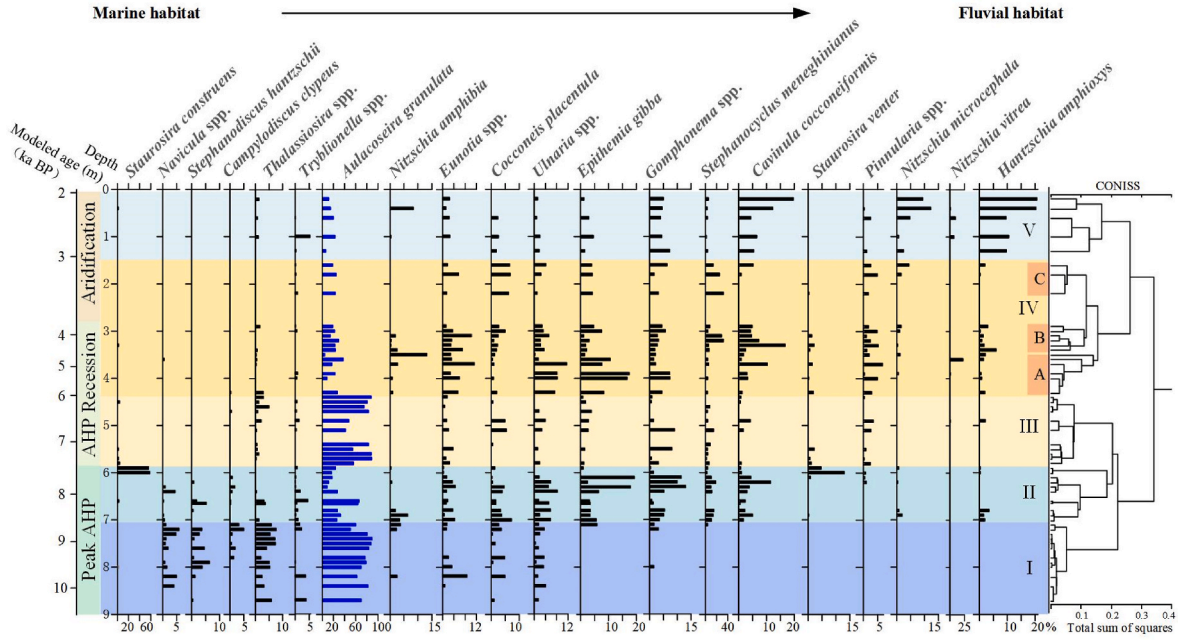

Fig. 5. CONISS-zoned diatom spectrum of B-1.

Assemblage I (below 7.0 m core depth, ca. >10.0-8.5 ka BP) was characterised by dominant fresh-brackish species *A. granulata*, as well as marine and brackish taxa, including *C. clypeus*, *Navicula* spp., *S. hantzschii*, *Thalassiosira* spp., and *Tryblionella* spp. Some low abundances of freshwater species such as *Ulnaria* spp. and *Eunotia* spp. were also observed (Fig. 5).

Assemblage II (7.0–5.9 m core depth, ca. 8.5-7.5 ka BP) witnessed a dramatic decrease in marine and brackish species, but an obvious increase in freshwater species in terms of both species' richness and abundance. Representative species included *E. gibba*, *S. meneghinianus*, *Gomphonema* spp., and *C. coccoeiformis* (Fig. 5).

Assemblage III (5.9–4.3 m core depth, ca. 7.5-6.0 ka BP) saw an increasing abundance of *A. granulata*. Comparatively, both marine and freshwater species became scarce (Fig. 5).

Assemblage IV (4.3–2.9 m core depth, 6.0-3.2 ka BP) persisted for a longer period, ca. 2000 years (Fig. 5). Freshwater species were dominant in both sub-units A and B, with a diverse range of species that alternately held the predominant position. When entering sub-unit C, the marine and brackish species almost disappeared, and freshwater-brackish taxa comprised only a small proportion with a low number of species, such as *A. granulata* and *C. placentula*. There was a hiatus of diatoms between B and C, lasting ca. 500 years (2.9–2.2 m core depth).

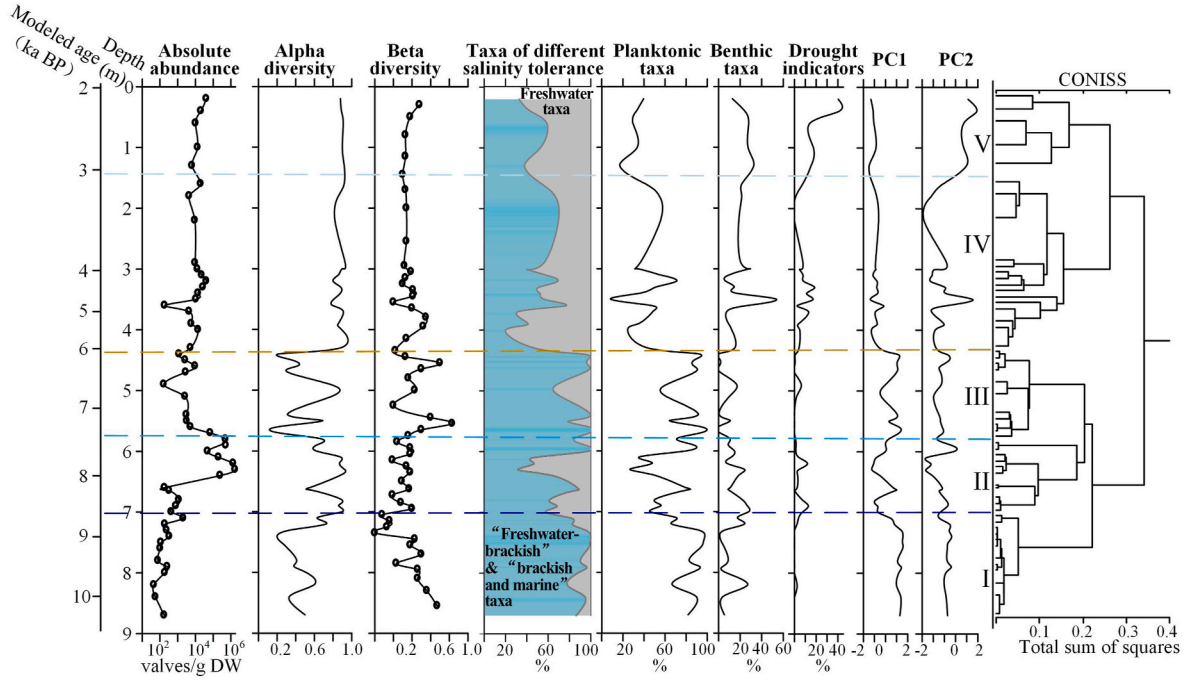

Fig. 6. CONISS diatom zonation of B-1, showing the temporal distribution of absolute abundances and species richness, Alpha/Beta diversities, freshwater and brackish-water sums and PC1 and PC2 (all discussed in the text).

Assemblage V (2.9–0.2 m core depth, 3.2-2.0 ka BP) showed an increasing dominance of freshwater species, such as *H. amphioxys* and *C. cocconeiformis*. Contemporaneously, a minor group of brackish and marine species coexisted (Fig. 5).

3.4. Distribution of diatom abundance and richness

The absolute abundance of diatom frustules ranged from 0.5×10^2 valves/g DW to 1.7×10^6 valves/g DW (Fig. 6), with the highest mean of 6.7×10^5 valves/g DW observed at a depth of 6.4–5.8 m (ca. 8.0–7.0 ka BP). By contrast, below the core depth of 6.6 m (ca. 8.0 ka BP), diatom frustule abundance was low, with a mean value of 4.0×10^2 valves/g DW.

There was a total of 149 diatom taxa identified, with the majority belonging to a wide variety of freshwater species (e.g. *Stephanocyclus meneghinianus*, *Cavinula cocconeiformis*, and *Epithemia gibba*) (S_Table 1 and Figs. 5 and 6). Due to the varying distribution of the predominant species *A. granulata*, accounting for >60% of the total, the richness pattern exhibited notable fluctuations (Figs. 5 and 6). Relatively low values, not exceeding 2.5, were mainly seen at core depths below 7.3 m, 5.4–6.1 m, and 4.4–4.7 m, corresponding to ca. 8.9 ka BP, ca. 7.7 - 7.1 ka BP, and ca. 6.5 - 6.1 ka BP, respectively. After ca. 6.0 ka BP (4.3 m core depth), the species composition of the diatom assemblage remained diverse. Variations in the alpha diversity were consistent with changes in the abundance of *A. granulata* (Fig. 6). According to pairwise dissimilarities detected by the beta diversity, when β_{sim} is closer to 1, the dissimilarity between the two assemblages becomes greater (Baselga, 2010; Socolar et al., 2016). Therefore, the apparent turnover reflected in B-1 appeared around 6.0 ka BP, when β_{sim} was >0.6. Also, planktonic communities remained remarkably high before ca. 6.0 ka BP, contrasting with a discernible moderate increase in benthic groups subsequent to this period (Fig. 6).

3.5. Classification of diatom taxa

A PCA was applied to the diatom dataset to further refine taxonomic classification and discern the primary modes of assemblage shift. The first axis (PCA1), accounting for 41.45% of the total variation, was primarily influenced by *A. granulata* and *S. hantzschii* with high positive loading, and *C. cocconeiformis* with high negative loading (Fig. 7). The TWINSPAN groups were also differentiated from each other in the PCA, reflected in their loadings on PC 1 and PC 2 (Fig. 6). Group 1, including most marine and brackish taxa, were loaded on the positive PC 1 axis (2.9772) while all the other groups, mainly with the freshwater communities, on the negative PC 1 axis (Figs. 4, 6 and 7). The majority of taxa within Groups 2–4 exhibit negative scores on both PC 1 and PC 2, placing them within the third quadrant of the PCA bi-plot. Conversely, Group 5 is distinguished by the highest positive loading on PC 2 (2.6325), concurrently featuring all drought-tolerant species (*C. cocconeiformis*, *N. amphibia*, and *H. amphioxys*) within the second quadrant (Figs. 4, 6 and 7).

The GAM response curves organised chronologically, delineated the rise and decline of taxa into three distinct types: geometric growth (Fig. 8a), gradient descent (Fig. 8b) and normal curve (Fig. 8c). The response curves indicated that the diatom assemblages were composed of dominant taxa with their population optimum in different periods. In the group of normal curves, the population peak of a particular taxon appeared either before or after 6.0 ka BP (Fig. 8c).

3.6. Diatom indicative species and their ecological habitats

3.6.1. Marine and brackish taxa

The diatom assemblages in core B-1 consist of brackish and marine taxa adapted to saline water, most of which were classified into Group 1 and, to a lesser extent, Group 2 (Fig. 4). Relative dominance is attributable to *Thalassiosira* spp., including *T. decipiens* and *T. symmetrica*, both oceanic and coastal planktonic species (Zalat and Vildary, 2007; Hammad and Ibrahim, 2012). The marine species *S. hantzschii* and *C. clypeus* are recorded in thalassic environments of the Nile lagoonal area (Zalat and Vildary, 2007). The former prefers relatively low temperature (Shafik et al., 1997) and the latter is adapted to living in shallow water as a large benthic species (Pankow, 1976). Other dominant saline taxa are *Navicula* spp. (such as *N. Lyrata* and *N. aegyptiaca*) and *Tryblionella* spp. (such as *T. scalaris*, *T. granulata*, *and T. punctata*), both commonly found in coastal lagoons and estuaries (Cholnoky, 1968; Foged, 1979; Zalat and Vildary, 2007).

3.6.2. Freshwater-brackish taxa

There are nine species in this group, mostly assigned to Group 5 (Fig. 4). Such species frequently live in freshwater (Fig. 4), although they are also found in brackish-water settings, such as estuaries, lagoons and coastal waters (Hällfors, 2004; Hassan et al., 2005; Zong et al., 2010;

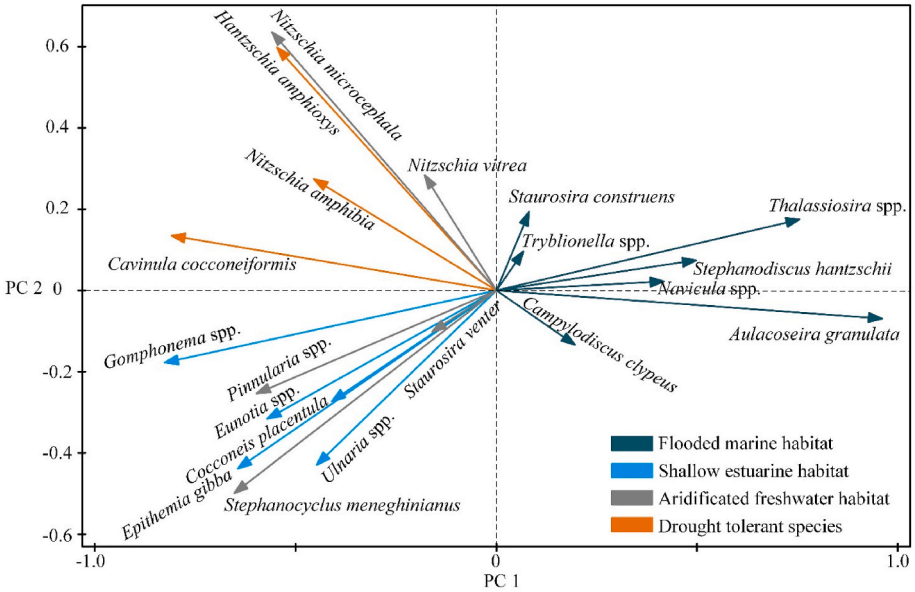

Fig. 7. PCA analysis of B-1.

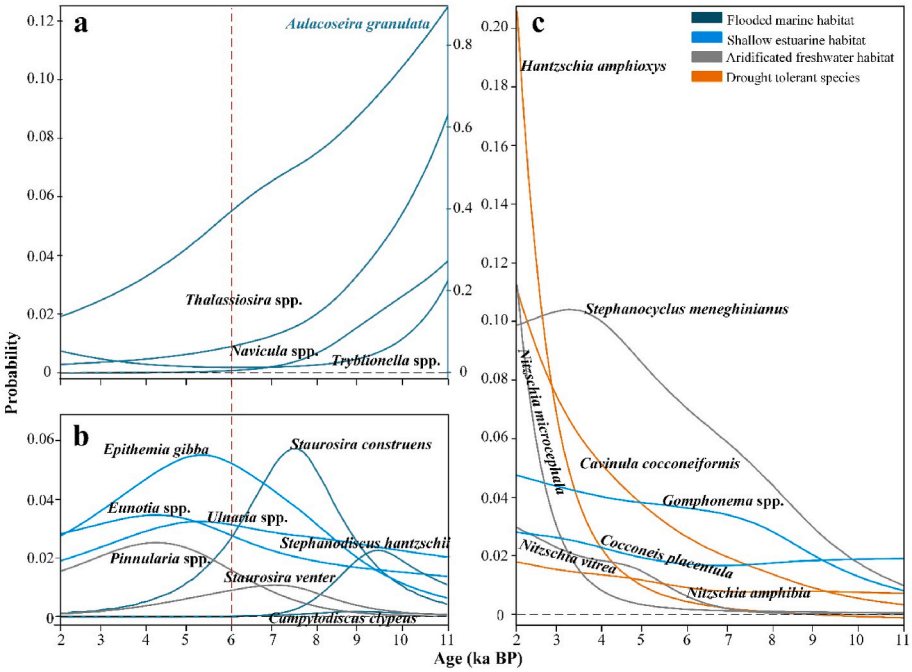

Fig. 8. GAM analysis of diatom taxa of B-1 and distribution patterns: a) descending; b) normal; c) ascending.

Lazrak et al., 2022). The representative species is *A. granulata*, predominant in B-1 assemblages (Figs. 4 and 5). Its relatively high dominance can be attributed to its competitive advantage in eutrophic to super-eutrophic waters. Therefore, *A. granulata* was widely used as a sensitive indicator of water areas of eutrophication and high productivity (Bicudo et al., 2016; Faustino et al., 2016) Particularly, *A. granulata* is identified as a characteristic Nile River diatom (Zalat, 2000), observed from upstream areas of both the Blue Nile and the White Nile, extending downstream to the estuary (Talling et al., 2009; Stager and Johnson, 2008; Hammad and Ibrahim, 2012). *A. granulata* frequently forms blooms in eutrophic waters (Kilham and Kilham, 1975; Campbell et al., 2006; Faustino et al., 2016).

3.6.3. Freshwater taxa

Throughout B-1, freshwater taxa from Groups 2–5 dominate (Fig. 4). The dominant freshwater species (Figs. 4 and 5) are characteristic of lakes, rivers and reservoirs, typically thriving in oligohalobous conditions, demonstrating tolerance to small amounts of salt. Amongst them, the genera *Pinnularia*, *Ulnaria*, *Eunotia* and *Gomphonema* exclusively comprise freshwater species (Foged, 1979; Van Dam et al., 1994). The dominant freshwater species, namely, *N. amphibia*, *H. amphioxys* and *C. cocconeiformis* are also recognised as drought indicators, since they dwell in either sand-soil or aerial and aeroterrestrial habitats (Van De Vijver et al., 2003; Zalat and Vildary, 2007; Cvetkoska et al., 2014; Maltsev et al., 2021). Meanwhile, primarily benthic and epiphytic, these freshwater taxa exhibit a preference for shallow environments owing to their phototropic response (Van Dam et al., 1994; Zalat and Vildary, 2007).

4. Discussion

Throughout the Holocene, the coastline of the north-central Nile Delta underwent significant changes, closely tied to the evolution of palaeo-Nile branches and the dynamic interplay between land and sea interactions (Fig. 1). The environment of B-1, further inland than the Burullus lagoon, was relatively stable, protected by the formation of a lagoon-barrier system on the seaward side (see Br-1 in Giaime et al., 2022) (Fig. 1), evidenced by its relatively stable sedimentation rate throughout the Holocene (Fig. 2). The diatom record of B-1 enabled us to reconstruct the Holocene hydroclimate changes, particularly in relation to marine invasion events (Figs. 3–5). Diatoms, being sensitive indicators of various environmental variables, offer valuable insights into these fluctuations (Hall and Smol, 1999; Bigler et al., 2003; Zalat and Vildary, 2007; Zalat, 2015).

4.1. Reconstructing Holocene hydroclimate-marine fluctuations

4.1.1. >10.0-8.5 ka BP: highest Nile flow and a diluted estuarine habitat

During the peak of the AHP, the highest abundance of *A. granulata* within assemblage I (prior to ca. 8.5 ka BP) was observed across B-1, alongside a notable presence of brackish and marine taxa from Group 1 (including *Thalassiosira* spp. and *S. hantzschii* etc.) (Figs. 4 and 5), consistent with the influx of significant volumes of Nile freshwater reaching the coastal areas. This period also corresponds to rapid rates of relative sea-level rise occurring during the Early Holocene (Fig. 3) (Stanley and Warne, 1993b), as recorded by the majority of the marine diatom communities (Figs. 4 and 5). Overall, it implies a brackish estuarine setting (Figs. 4 and 5), but high abundances of *A. Granulata* suggest that the estuarine waters were significantly diluted by the substantial influx of Nile floodwaters rich in terrestrial nutrients. These conditions facilitated the formation of algal blooms in eutrophic environments (Faustino et al., 2016; Bicudo et al., 2016).

4.1.2. ca. 8.5-7.5 ka BP: brief waning of Nile flow and oligotrophic habitat

The sharp decline of *A. granulata* (assemblage II; ca. 8.5-7.5 ka BP) indicates the waning of Nile flow (Fig. 5), which was closely associated with the retreat of the Intertropical Convergence Zone (ITCZ) during the later AHP peak (Tierney et al., 2011; Shanahan et al., 2015; Castañeda et al., 2016; Liu et al., 2017). Meanwhile, the flourishing freshwater taxa belonging to Groups 2–4 and assemblage II (Figs. 4 and 5), including species such as *Eunotia* spp., *E. gibba* and *Gomphonema* spp., suggest that the estuarine habitat was characterised by shallower water settings and lower nutrient concentrations, indicative of oligotrophic conditions (Patrick and Reimer, 1975; Floener and Bothe, 1980; Van Dam et al., 1994; Zalat and Vildary, 2007; Pavlov and Levkov, 2013). In comparison, reduced brackish and marine taxa in assemblage II attest to less

marine influence on the Nile coast during this period, although rapid sea-level rise did not slow until ca. 5 ka BP (Fig. 3; Giaime et al., 2022). Between, 8.5-7.5 ka BP RSL was around 10 m below present MSL and RSL rising rates were relatively modest at around 0.5 mm/yr. As fluvial input continued, the abundance and diversity of freshwater species increased during the later stage of the AHP peak (Figs. 5 and 6), reflecting a shift in the dominant influence from marine to freshwater (Arbouille and Stanley, 1991; Giaime et al., 2022).

4.1.3. ca. 7.5–6.0 ka BP: unstable Nile flow and fluctuating salinity levels in the estuarine habitat

This period saw two major pulses of *A. granulata* in diatom assemblage III (Fig. 5), with a low occurrence between ca. 7.0–7.4 ka BP., reflecting unstable hydroclimate conditions in the upper Nile watershed following a further decline of the AHP (Tierney et al., 2011; Wang et al., 2022). Studies by Tierney et al. (2011) and Shanahan et al. (2015) found that higher Nile freshwater levels during this period were associated with the transition from the AHP peak to the early stages of the AHP recession as the ITCZ migrated southwards. This caused marked fluctuations in precipitation over the Ethiopian Highlands due to strong interaction between the African and Indian monsoons (Castañeda et al., 2016; Liu et al., 2017). Also, an eastward shift in the Congo Air Boundary (CAB) during this period intensified the unstable hydroclimate conditions over the eastern African plateau (Castañeda et al., 2016; Liu et al., 2017). In addition, the decline of freshwater diatom species (*E. gibba*, *Gomphonena* spp., and *Eunotia* spp., etc.) in Group 3 and assemblage III suggests a shallowing estuarine environment, where benthic communities faced increased difficulty in adapting. Several brackish diatoms disappeared as the delta coastline prograded seawards due to high fluvial sediment supply and the creation of new accommodation driven by RSL rise (Stanley and Warne, 1993a; Giaime et al., 2022, Fig. 3).

4.1.4. ca. 6.0–3. 2 ka BP: delta progradation and a drying coastal habitat

After 6.0 ka BP, RSL stabilised with rising rates between 0 and 1.5 mm/yr during the following period (Fig. 3). The diatom assemblage IV saw a ca. 50% reduction in *A. granulata* compared to previous assemblages, but also marked the reappearance of freshwater communities from Groups 2–4 (Fig. 4). This was related to the drying climate of the Nile basin (Wang et al., 2022; Zhang et al., 2022), confirmed by the contrasting trends of *A. granulata* (increase) and *E. gibba* (decrease) during the late period of the AHP recession after approximately 6 ka BP (Zalat and Vildary, 2007). Also, the appearance of sporadic fresh-brackish taxa from Group 5 is consistent saline coastal habitats due to high evaporation under post-AHP drying climate conditions (Figs. 4 and 5). The discontinuous occurrence of diatoms probably translates an "extreme aridity" event around 3.2 ka BP (Fig. 5). As the ITCZ moved further southward, Nile floods decreased significantly (Fig. 9b–g).

4.1.5. ca. 3.2-2.0 ka BP: intensifying aridification

This period witnessed a marked increase in drought-indicative species (15–20% of total), mainly *N. amphibia, H. amphioxys*, and *C. cocconeiformis* of Group 5 and the assemblage V (Figs. 4 and 5), consistent with an intensified arid climate of the Nile River basin. Unlike before, the Buto coast was seldom flooded by Nile flow (Giaime et al., 2022; Wang et al., 2022). *H. amphioxys* and *C. cocconeiformis*, both characterised as being aerial diatoms (Cvetkoska et al., 2014; Jahn et al., 2014), flourished in the extremely dry environment of the Buto coast, with blooms of up to 20%. These diatoms are even capable of living in soil and beach sand, and, in a context of RSL stability, they record the environmental change from a former lagoon coast to a coastal plain (Giaime et al., 2022).

4.2. 6.0 ka BP: timing of saline to arid habitat transformation

Our PCA analysis of the diatom assemblages revealed that salinity

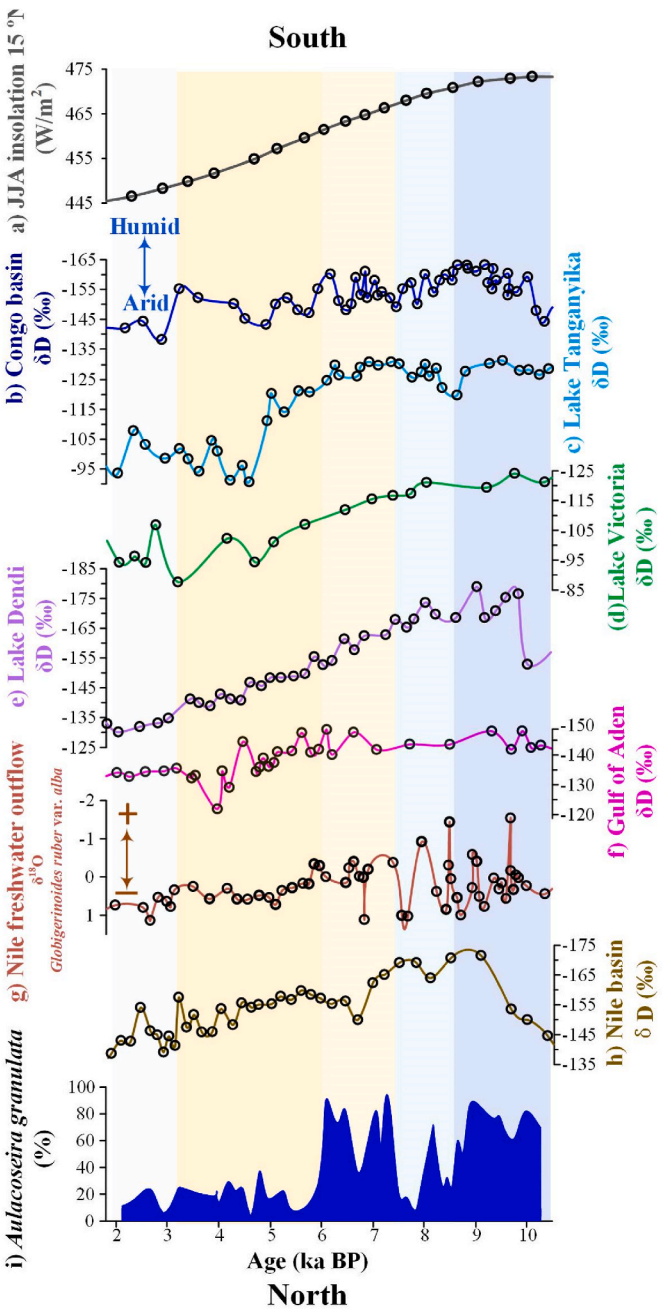

Fig. 9. Hydroclimate fluctuations of the Nile River basin. Comparison of the Nile flow indicator *Aulacoseira granulata* of B-1 with other basin-wide hydroclimate proxies: a) Summer insolation (June, July and August) at 25° N (Laskar et al., 2004); b) Congo Basin δD_{wax} (Schefuß et al., 2005); c) Lake Tanganyika δD_{wax} (Tierney et al., 2008); d) Lake Victoria δD_{wax} (Berke et al., 2012); e) δD values of the n-C29 from Lake Dendi sediment core (Jaeschke et al., 2020); f) Gulf of Aden δD_{wax} (Tierney and de Menocal, 2013); g) $d^{18}O$ data of the core MS27PT (Revel et al., 2015); h) Nile Basin δD_{wax} (Castañeda et al., 2016); i) Relative abundances of *Aulacoseira granulata* of B-1. δD values from the Nile and Congo River Basins were determined using C31 n-alkane (Schefuß et al., 2005; Castañeda et al., 2016), whereas δD measurements for the Gulf of Aden, Lake Tanganyika and Lake Victoria were conducted using C28 (Tierney et al., 2008; Berke et al., 2012; Tierney and de Menocal, 2013).

variations affected by Nile flow played a key role in controlling the eco-environmental evolution of the Buto coast throughout the Holocene. As shown in the coordinate graph (Figs. 4, 6 and 7), all "brackish and marine" taxa exhibited positive loading on PC1, while freshwater taxa were negatively loaded. The proportion of drought-tolerant species not

only consistently varied with PC2 (Figs. 4, 6 and 7), but also exhibited a positive loading on PC2 (Figs. 4, 6 and 7). Apparently, "freshwater-brackish" and "brackish and marine" taxa varied proportionally with freshwater taxa (Fig. 6). The transition from brackish-marine to freshwater dominance occurred ca. 6.0 ka BP (Figs. 5 and 6). There was an apparent increase in both the quantity and diversity of freshwater taxa after 6.0 ka BP (Figs. 5 and 6), indicating fluvial inputs into a dominant estuarine eco-setting (Arbouille and Stanley, 1991; Giaime et al., 2022). The oscillation between planktonic and benthic proportions (Fig. 6), further corroborates the dominance of estuarine habitats influenced by high Nile floods before 6.0 ka BP. Subsequently, a notable shift occurred whereby land surface processes began to exert a prevailing influence. In the meantime, increases in drought-tolerant species (*N. amphibia*, *H. amphioxys*, and *C. cocconeiformis*) demonstrates that the post-AHP drying hydroclimate prevailed throughout the river basin (Figs. 5–7) (Castañeda et al., 2016).

The importance of the temporal inflection point at ca. 6.0 ka BP was also expressed in the GAM and diversity analyses (Fig. 8a, b, c). The brackish and marine taxa of Group 1 (Fig. 4) exhibited a descending trend but eventually stabilised at low relative abundances after 6.0 ka BP (Fig. 8a), whereas the drought-indicative species displayed a notable increase after 6.0 ka BP. (Fig. 8c). In the type of normal distribution, all freshwater taxa within Groups 2–3 reached their peak abundance after 6.0 ka BP (Fig. 8b). Both the variation of D_α and β_{sim} also identified the significant transformation after 6.0 ka BP. From >10.0-6.0 ka BP, the diversity variation pattern remained consistent alongside changes in the proportion of taxa with varying salinity tolerance (Fig. 6). Since 6.0 ka BP, the persistent high values of D_α coupled with low β_{sim} values (Fig. 6) suggests that the freshwater environment had sufficiently stabilised, allowing the diatom community to maintain a consistently high and steady diversity.

It is worth mentioning that the timing of the habitat transformation ca. 6.0 ka BP in B-1 coincides with both RSL stability and with the establishment of the settlement of Buto, precisely after 6.0 ka BP. This chronological correlation underscores the significance of Buto settlement in the context of the predynastic Buto Culture of Egypt, serving as a crucial link between Upper and the Lower Egypt societies (Mączyńska, 2014).

4.3. Diagnostic diatom taxa: implications for hydroclimate events

Diagnostic diatom communities were associated with specific hydroclimate events. Higher abundances of *S. meneghinianus* ca. 8.5 ka BP, 7.8 ka BP and 4.2 ka BP (Fig. 5) may also reflect an estuarine setting richer in nutrients, given its competitive edge in eutrophic waters (B-Béres et al., 2014; Fontana et al., 2014; Faustino et al., 2016). The remarkably high abundances of *E. gibba* and *Gomphonema* spp. ca. 7.8 ka BP and 6.4 ka BP (Fig. 5) point to more oligotrophic conditions (Zalat and El-Sheekh, 1999; Adler et al., 2014; Cvetkoska et al., 2014; Glushchenkoa and Kulikovskiyb, 2017).

S. construens and *S. venter* are small sized (3–20 μm) benthic/tychoplanktonic species (Morales, 2001), most common in coastal settings (De Wolf, 1982; Vos and De Wolf, 1993). The higher abundances of *S. construens* >50% ca. 7.6 ka BP (Fig. 5) probably indicates increasing marine processes in a context of high RSL rising rates (Vos and De Wolf, 1993; Hassan et al., 2003), when the Nile flow was lower (seeing lower *A. granulata* of Fig. 5). The high abundance of *S. construens* is likely a result of taphonomic processes rather than ecological attributes (Hassan et al., 2005). Its frustules are easily accumulated in high concentrations through tidal transport processes.

4.4. Aulacoseira granulata: Nile flow indicator

A. granulata is a widespread centric and planktonic diatom, blooming in freshwater lakes, reservoirs and rivers (Kilham and Kilham, 1975; Costa et al., 2009). It can also follow the outflow of freshwater into brackish estuarine, lagoonal and coastal settings (Shen et al., 1995; Odebrecht et al., 2005; Hassan, 2010; Zong et al., 2010). Some studies have classified it as a brackish species (e.g. Huang et al., 2004; Zong et al., 2010). However, as a typical freshwater species only tolerant to low salinity, its abundance and distribution obviously displayed a negative correlation with salinity (Huang et al., 2004; Zong et al., 2010), but a positive correlation with runoff discharge (Costa et al., 2009). Previous studies have recognised *A. granulata* as a Nile flow indicator (Zalat, 2000; Williams et al., 2010), with a wide latitudinal range, from the Blue Nile and White Nile to downstream and estuarine areas (Stager and Johnson, 2008; Talling et al., 2009; Hammad and Ibrahim, 2012). Our analysis demonstrates that the Holocene abundances of *A. granulata* in B-1 are significantly correlated to the hydroclimate dynamics of the Nile basin (Fig. 9a–i). In light of these observations, we suggest that *A. granulata* serve as a palaeo-Nile flow proxy. Its proportion of total taxa ranging from 60 to 80% during the Early Holocene to ca. 20% during the Late Holocene, supporting the estimation that the palaeo-Nile flow ca. 8000 years ago was approximately three times greater than that of the recent past (Figs. 5 and 9i). A similar estimate of palaeo-Nile flow during the AHP can be also inferred from sedimentation patterns off the Nile coast (Vadsaria et al., 2019; Zaki et al., 2021; Blanchet et al., 2024), and the unique pollen species (Nile headwater indicators) derived from the upper Nile source (seeing Figs. 5 and 6 of Zhao et al., 2020).

5. Conclusions

This study has demonstrated that.

(1) *Aulacoseira granulata* is a sensitive freshwater-brackish diatom species, which fluctuated in proportion to Nile flow throughout the Holocene, making it a reliable proxy for reconstructing past Nile flow.
(2) The ^{14}C-dated diatom spectra show that 6.0 ka BP was a key change point, marking the transition from a Nile-influenced estuary to a freshwater-dominated setting, corresponding to the shift from the peak AHP to the subsequent aridification phase and a stabilisation of relative sea level.
(3) 5 diatom assemblages were elucidated in this study. Assemblage I (ca. >10.0-8.5 ka BP) exhibited the highest abundance of *A. granulata* (80-60%) alongside marine taxa, indicating a diluted estuarine environment during the Holocene marine transgression and the peak of the AHP. The subsequent lowering of *A. granulata* (to 20–40%) in assemblage II (ca. 8.5-7.5 ka BP) saw an incipient decrease in Nile flow during the latter phases of the AHP. Assemblage III (ca. 7.5-6.0 ka BP) witnessed fluctuations in *A. granulata* (50–80%) and no marine taxa, reflecting unstable Nile flow caused by monsoon hydro-dynamics in eastern Africa in response to the southerly migration of the ITCZ. After 6.0 ka BP, Nile flow decreased further (*A. granulata* to 20–30%), leading to a more oligohalobous coastal habitat under the persistent drying climate (assemblage IV). The drought-tolerant diatom communities of assemblage V (3.2 ka BP onward) are consistent with basin-wide aridification.
(4) Higher abundances of the drought-tolerant taxa *Nitzschia amphibia, Hantzschia amphioxys* and *Cavinula cocconeiformis* are consistent with climate aridity during both the late period of 4.0 ka BP and 3.0 ka BP. The sudden increase in abundance of small species such as *Staurosira construens* and *Staurosira venter* suggests intense tidal dynamics along the estuarine coast ca. 7.6 ka BP, a period coinciding with diminished Nile flow intensity. High abundances of *E. gibba* ca. 7.3-6.0 ka BP and 5.3 ka BP suggests that the estuarine habitat exhibited markedly oligohaline conditions during these periods.

Authors individual contributions

Y. Wang, X. Zhao, Z. Chen, A. Salem designed the project. Y. Wang, X. Zhao, Z. Chen, A. Salem., and J. Chen collected sediment sample; Y. Wang and J. Zhou identified diatoms. X. Zhao and Z. Chen worked for AMS-dating materials; Y. Wang, X. Zhao, N. Marriner, D. Kaniewski, and Z. Chen wrote the manuscript, and all individuals participated in discussion and agreed this submission.

Declaration of competing interest

The authors declare that they have no known competing financial interests or personal relationships that could have appeared to influence the work reported in this paper.

Acknowledgements

The authors are grateful to professor Yongqiang Zong, whose constructive suggestions improved the quality of this manuscript. The authors are also greatly indebted to the University of Kafrelsheikh, Egypt for providing logistical and scientific support during fieldwork. The project was financially supported by the China National Natural Science Foundation (Grant No. 42106161; 42261144741).

Appendix A. Supplementary data

Supplementary data to this article can be found online at https://doi.org/10.1016/j.quascirev.2024.109070.

Data availability

Data will be made available on request.

References

Adler, S., Trapp, E.M., Dede, C., Maier, U.G., Zauner, S., 2014. Rhopalodia gibba: the first steps in the birth of a novel organelle? Endosymbiosis 167–179.
Arbouille, D., Stanley, D.J., 1991. Late quaternary evolution of the Burullus lagoon region, north-central Nile Delta, Egypt. Mar. Geol. 99 (1–2), 45–66.
B-Béres, V., Török, P., Kókai, Z., Krasznai, E.T., Tóthmérész, B., Bacsi, I., 2014. Ecological diatom guilds are useful but not sensitive enough as indicators of extremely changing water regimes. Hydrobiologia 738, 191–204.
Baselga, A., 2010. Partitioning the turnover and nestedness components of beta diversity. Global Ecol. Biogeogr. 19 (1), 134–143.
Battarbee, R.W., Jones, V.J., Flower, R.J., Cameron, N.G., Bennion, H., Carvalho, L., Juggins, S., 2001. Diatoms. In: Smol, J.P., Birks, H.J.B., Last, W.M., Bradley, R.S., Alverson, K. (Eds.), Tracking Environmental Change Using Lake Sediments. Kluwer Academic Publishers, Dordrecht, pp. 155–203.
Berke, M.A., Johnson, T.C., Werne, J.P., Grice, K., Schouten, S., Sinninghe Damsté, J.S., 2012. Molecular records of climate variability and vegetation response since the late pleistocene in the Lake Victoria basin, east Africa. Quat. Sci. Rev. 55, 59–74.
Bernhardt, C.E., Horton, B.P., Stanley, D.J., 2012. Nile Delta vegetation response to Holocene climate variability. Geology 40, 615–618.
Bicudo, D.C., Tremarin, P.I., Almeida, P.D., Zorzal-Almeida, S., Wengrat, S., Faustino, S. B., Costa, L.F., Bartozek, E.C.R., Rocha, A.C.R., Bicudo, C.E.M., Morales, E.A., 2016. Ecology and distribution of Aulacoseira species (Bacillariophyta) in tropical reservoirs from Brazil. Diatom Res. 31 (3), 199–215. https://doi.org/10.1080/0269249X.2016.1227376.
Bigler, C., Grahn, E., Larocque, I., Jeziorski, A., Hall, R., 2003. Holocene environmental change at Lake Njulla (999 m a.s.l.), northern Sweden: a comparison with four small nearby lakes along an altitudinal gradient. J. Paleolimnol. 29, 13e29.
Blaauw, M., Christen, J.A., 2011. Flexible paleoclimate age-depth models using an autoregressive gamma process. Bayesian Anal 6, 457–474.
Blanchet, C.L., Ramisch, A., Tjallingii, R., Ionita, M., Laruelle, L., Bagge, M., Volker Klemann, V., Brauer, A., 2024. Climatic pacing of extreme nile floods during the north African Humid Period. Nat. Geosci. 17, 638–644.
Box, M.R., Krom, M., Cliff, R., Bar-Matthews, M., Almogi-Labin, A., Ayalon, A., Paterne, M., 2011. Response of the Nile and its catchment to millennial-scale climatic change since the LGM from Sr isotopes and major elements of East Mediterranean sediments. Quat. Sci. Rev. 30, 431–442.
Butzer, K.W., 1976. Early Hydraulic Civilization in Egypt: A Study in Cultural Ecology. University of Chicago Press, Chicago.
Cahill, N., Kemp, A.C., Horton, B.P., Parnell, A.C., 2016. A Bayesian hierarchical model for reconstructing relative sea level: from raw data to rates of change. Clim. Past 12, 525–542.
Campbell, I., Poole, C., Giesen, W., Valbo-Jorgensen, J., 2006. Species diversity and ecology of tonle sap Great Lake, Cambodia. Aquat. Sci. 68, 355–373.
Carvalho do Amaral, P.G., Fonseca Giannini, P.C., Sylvestre, F., Ruiz Pessenda, L.C., 2012. Paleoenvironmental reconstruction of a Late Quaternary lagoon system in southern Brazil (Jaguaruna region, Santa Catarina state) based on multi-proxy analysis. J. Quat. Sci. 27 (2), 181–191.
Castañeda, I.S., Schouten, S., Patzold, J., Lucassen, F., Kasemann, S., Kuhlmann, H., Schefuß, E., 2016. Hydroclimate variability in the nile River Basin during the past 28,000 years. Earth Planet Sci. Lett. 438, 47–56.
Cholnoky, B.J., 1968. Die Okologie der Diatomeen in Binnengewassern. Lehre J Cramer Verlag, Berlin, p. 699.
Costa, L.S., Huszar, V.L.M., Ovalle, A.R., 2009. Phytoplankton functional groups in a tropical estuary: hydrological control and nutrient limitation. Estuar. Coast 32, 508–521.
Cvetkoska, A., Levkov, Z., Hamilton, P.B., Potapova, M., 2014. The biogeographic distribution of Cavinula (Bacillariophyceae) in North America with the descriptions of two new species. Phytotaxa 184 (4), 181–207.
De Wolf, H., 1982. Method of coding of ecological data from diatoms for computer utilization. Med. Rijks Geol. Dienst. 36, 95–99.
deMenocal, P., Ortiz, J., Guilderson, T., Adkins, J., Sarnthein, M., Baker, L., Yarusinsky, M., 2000. Abrupt onset and termination of the African Humid Period: rapid climate responses to gradual insolation forcing. Quat. Sci. Rev. 19 (1–5), 347–361.
Emeis, K.C., Struck, U., Schulz, H.M., Rosenberg, R., Bernasconi, S., Erlenkeuser, H., Sakamoto, T., Martinez-Ruiz, F., 2000. Temperature and salinity variations of Mediterranean Sea surface waters over the last 16,000 years from records of planktonic stable oxygen isotopes and alkenone unsaturation ratios. Palaeogeogr. Palaeoclimatol. Palaeoecol. 158, 259–280.
Emeis, K.C., Schulz, H., Struck, U., Rossignol-Strick, M., Erlenkeuser, H., Howell, M., Kroon, D., Mackensen, A., Ishizuka, S., Oba, T., 2003. Eastern Mediterranean surface water temperatures and $\delta^{18}O$ composition during deposition of sapropels in the late Quaternary. Paleoceanography 18, 1005.
Espinosa, M.A., Fayó, R., Vélez-Agudelo, C., 2022. Diatom-based paleoenvironmental reconstruction from the coast of Northern Patagonia, Argentina. J. S. Am. Earth Sci., 103874
Faustino, S.B., Fontana, L., Bartozek, E.C.R., Bicudo, C.E.D.M., Bicudo, D.D.C., 2016. Composition and distribution of diatom assemblages from core and surface sediments of a water supply reservoir in Southeastern Brazil. Biota Neotropica 16 (2), e20150129.
Floener, L., Bothe, H., 1980. Nitorgen fixation in Rhopalodia gibba, a diatom containing blue-greenish inclusions symbiotically. In: Schwemmler, W., Schenk, H.E.A. (Eds.), Endocytobiology, Endosymbiosis and Cell Biology. Walter de Gruyter & Co., Berlin, pp. 541–552.
Foged, N., 1979. Diatoms in New Zealand, the north Island. Bibl. Phycol. 47, 1–225.
Fontana, L., Albuquerque, A.L.S., Brenner, M., Bonotto, D.M., Sabaris, T.P., Pires, M.A.F., Cotrim, M.E.B., Bicudo, D.C., 2014. The eutrophication history of a tropical water supply reservoir in Brazil. J. Paleolimnol. 51, 29–43.
Giaime, M., Salem, A., Wang, Y., Zhao, X., Liu, Y., Chen, J., Sun, Q., Shama, A.A., Elhossainy, M., Morhange, C., 2022. Holocene evolution and signature of environmental change of the Burullus lagoon (Nile Delta) deciphered from a long sediment record. Palaeogeogr. Palaeoclimatol. Palaeoecol. 590, 110861.
Glushchenko, A.M., Kulikovskiy, M.S., 2017. Taxonomy and distribution of the genus Eunotia Ehrenberg in aquatic ecosystems of Vietnam. Inland water biology 10, 130–139.
Grimm, E.C., 1987. CONISS: a FORTRAN 77 program for stratigraphically constrained cluster analysis by the method of incremental sum of squares. Comput. Geosci. 13 (1), 13–35.
Hall, R.I., Smol, J.P., 1999. Diatoms as indicators of lake eutrophication. In: Stoermer, E. F., Smol, J.P. (Eds.), The Diatoms: Applications for the Environmental and Earth Sciences. Cambridge University Press, p. 128e168.
Hällfors, G., 2004. Checklist of Baltic sea phytoplankton species, Balt. Sea. Environ. Proc. 95, 5–208.
Hammad, D.M., Ibrahim, L.A., 2012. Influence of iron and silicon speciation on the abundance of diatoms in River Nile. J. Appl. Sci. Res. 8 (1), 556–570.
Hassan, G., 2010. Paleoecological significance of diatoms in Argentinean estuaries: what do they tell us about the environment? In: Crane, J.R., Solomon, A.E. (Eds.), Estuaries: Types, Movement Patterns and Climatical Impacts. Nova Science Publishers, New York, pp. 71–147.
Hassan, G., Espinosa, M.A., Isla, F.I., 2003. Diatomeas bentonicas de la albufera Mar Chiquita (Buenos Aires, Argentina): Consideraciones tafonomicas preliminares. Ameghiniana Suplemento Resumenes 40, 102R–103R.
Hassan, H., Anis, M., Elmasry, M., 2005. MOS current mode circuits: analysis, design, and variability. IEEE Trans. Very Large Scale Integr. Syst. 13 (8), 885–898.
Hastie, T.J., Tibshirani, R., 1990. Generalized Additive Models. Chapman & Hall, London, U.K.
Heaton, T.J., Kohler, P., Butzin, M., Bard, E., Reimer, R.W., Austin, W.E., Ramsey, C.B., Grootes, P.M., Hughen, K.A., Kromer, B., 2020. Marine20-the marine radiocarbon age calibration curve (0-55,000 cal BP). Radiocarbon 62 (4), 779–820.
Hill, M.O., Šmilauer, P., 2005. TWINSPAN for Windows Version 2.3. Centre for Ecology and Hydrology & University of South Bohemia, Huntingdon & Ceske Budejovice.
Huang, L., Jian, W., Song, X., Huang, X., Liu, S., Qian, P., Yin, K.D., Wu, M., 2004. Species diversity and distribution for phytoplankton of the Pearl River estuary during rainy and dry seasons. Mar. Pollut. Bull. 49 (7–8), 588–596.
Jaeschke, A., Thienemann, M., Schefuss, E., Urban, J., Schaebitz, F., Wagner, B., Rethemeyer, J., 2020. Holocene hydroclimate variability and vegetation response in the Ethiopian Highlands (Lake Dendi). Front. Earth Sci. 8, 585770.

Jahn, R., Kusber, W.H., Lange-Bertalot, H., 2014. Typification and taxonomy of Hantzschia amphioxys (Ehrenberg) Grunow (Bacillariophyta): type of the genus name Hantzschia Grunow. Nova Hedwigia, Beiheft 143, 103–110.
Katoh, K., 1993. Deletion of less-abundant species from ecological data. Diatom 8, 1–5.
Kilham, S.S., Kilham, P., 1975. Melosira granulata (Ehr) Ralfs, morphology and ecology of a cosmopolitan freshwater diatom. Verh. Int. Ver. Limnol. 19, 2716–2721.
Koutsodendris, A., Brauer, A., Reed, J.M., Plessen, B., Friedrich, O., Hennrich, B., Zacharias, I., Pross, J., 2017. Climate variability in SE Europe since 1450 ad based on a varved sediment record from Eetoliko Lagoon (Western Greece). Quat. Sci. Rev. 159, 63–76.
Krom, M.D., Stanley, J.D., Cliff, R.A., Woodward, J.C., 2002. Nile River sediment fluctuations over the past 7000 yr and their key role in sapropel development. Geology 30, 71–74.
Laskar, J., Robutel, P., Joutel, F., Gastineau, M., Correia, A.C., Levrard, B., 2004. A long-term numerical solution for the insolation quantities of the Earth. Astron. Astrophys. 428 (1), 261–285.
Lazrak, K., Tazart, Z., Berger, E., Mouhri, K., Loudiki, M., 2022. Spatial variation in benthic diatom communities in relation to salinity in the arid drâa river basin (southern Morocco). Appl. Ecol. Environ. Res. 20 (5), 3709–3736.
Liu, X.T., Rendle-Bühring, R., Kuhlmann, H., Li, A., 2017. Two phases of the Holocene East African Humid Period: inferred from a high-resolution geochemical record off Tanzania. Earth Planet Sci. Lett. 460, 123–134.
Macklin, M.G., Lewin, J., Woodward, J.C., 2012. The fluvial record of climate change. Phil. Trans. Math. Phys. Eng. Sci. 370 (1966), 2143–2172.
Mączyńska, A., 2014. The Nile Delta as a center of cultural interaction between upper Egypt and the southern levant in the 4th millennium BC. Stu. Anc. Art Civiliz. 18, 25–45.
Maltsev, Y., Maltseva, K., Kulikovskiy, M., Maltseva, S., 2021. Influence of light conditions on microalgae growth and content of lipids, carotenoids, and fatty acid composition. Biology 10 (10), 1060.
Marriner, N., Flaux, C., Morhange, C., Stanley, J.D., 2013. Tracking Nile Delta vulnerability to Holocene change. PLoS One. 8 (7), e69195. https://doi.org/10.1371/journal.pone.0069195.
Marriner, N., Kaniewski, D., Pourkerman, M., Vacchi, M., Melini, D., Seeliger, M., Morhange, C., Spada, G., 2023. Forecasted weakening of Atlantic overturning circulation could amplify future relative sea-level rise in the Mediterranean: a review of climate and tide-gauge data links. Earth Sci. Rev. 242, 104456. https://doi.org/10.1016/j.earscirev.2023.104456.
Marshall, M.H., Lamb, H.F., Huws, D., Davies, S.J., Bates, R., Bloemendal, J., Boyle, J., Leng, M.J., Umer, M., Bryant, C., 2011. Late pleistocene and Holocene drought events at lake tana, the source of the blue nile. Glob. Planet. Chang. 78, 147–161.
McQuoid, M.R., Hobson, L.A., 2001. A Holocene record of diatom and silicoflagellate microfossils in sediments of Saanich Inlet, ODP Leg 169S. Mar. Geol. 174 (1–4), 111–123.
Morales, E.A., 2001. Morphological studies in selected fragilarioid diatoms (Bacillariophyceae) from Connecticut waters (USA). Proc. Acad. Nat. Sci. Phila. 151 (1), 105–120.
Muylaert, K., Sabbe, K., Vyverman, W., 2009. Changes in phytoplankton diversity and community composition along the salinity gradient of the Schelde estuary (Belgium/The Netherlands). Estuar. Coast Shelf Sci. 82 (2), 335–340.
Nakanishi, T., Hong, W., Sung, K.S., Nakashima, R., Nahm, W.H., Lim, J., Katsuki, K., 2017. Offset in radiocarbon age between plant and shell pairs in Holocene sediment around the Mae-ho Lagoon on the eastern coast of Korea. Quat. Int. 447, 3–12.
Odebrecht, C., Abreu, P.C., et al., 2005. Drought effects on pelagic properties in the shallow and turbid Patos Lagoon, Brazil. Estuaries 28, 675–685.
Pankow, H., 1976. Algenflora der Ostsee. II. Plankton. Stuttgart (Verlag Fischer), p. 493.
Patrick, R., Reimer, C.W., 1975. The diatoms of the United States. Vol. II, Pt. I. Acad. Nat. Sci. Phil., Monograph 13.
Pausata, F.S.R., Gaetani, M., Messori, G., Berg, A., de Souza, D.M., Sage, R.F., de Menocal, P.B., 2020. The greening of the sahara: past changes and future implications. One Earth 2 (3), 235–250.
Pavlov, A., Levkov, Z., 2013. Diversity and distribution of taxa in the genus Eunotia ehrenberg (bacillariophyta) in Macedonia. Phytotaxa 86 (1), 1–117.
Reimer, P.J., Austin, W.E., Bard, E., Bayliss, A., Blackwell, P.G., Ramsey, C.B., Butzin, M., Cheng, H., Edwards, R.L., Friedrich, M., 2020. The IntCal20 Northern Hemisphere radiocarbon age calibration curve (0–55 cal kBP). Radiocarbon 62, 725–757.
Renberg, I., 1990. A procedure for preparing large sets of diatom slides from sediment cores. J. Paleolimnol. 4 (1), 87–90.
Revel, M., Ducassou, E., Skonieczny, C., Colin, C., Bastian, L., Bosch, D., et al., 2015. 20,000 years of Nile River dynamics and environmental changes in the Nile catchment area as inferred from Nile upper continental slope sediments. Quat. Sci. Rev. 130, 200–221.
Rossignol-Strick, M., 1983. African monsoons, an immediate climate response to orbital insolation. Nature 304, 46–49.
Said, R., 1981. The Geological Evolution of the River Nile. Springer-Verlag, New York.
Schallenberg, M., Saulnier-Talbot, É., 2014. Recent Environmental History of Wainono Lagoon (South Canterbury, New Zealand). Environment Canterbury, Christchurch. Report No. R14/48.
Schefuß, E., Schouten, S., Schneider, R.R., 2005. Climatic controls on central African hydrology during the past 20,000 years. Nature 437 (7061), 1003–1006.
Shafik, H.M., Herodek, S., Vörös, L., Présing, M., Kiss, K.T., 1997. Growth of Cyclotella meneghiniana Kutz. I. Effects of temperature, light and low rate of nutrient supply. In Annales de Limnologie-International Journal of Limnology 33 (3), 139–147. EDP Sciences.
Shanahan, T.M., McKay, N.P., Hughen, K.A., Overpeck, J.T., Otto-Bliesner, B., Heil, C.W., King, J., Scholz, C.A., Peck, J., 2015. The time-transgressive termination of the african Humid Period. Nat. Geosci. 8, 140–144.
Shen, H., Xu, R., Wang, G., 1995. Studies on phytoplankton in waters adjacent to islands of Shanghai. Mar. Sci. Bull. 14, 26–37 (in Chinese with English abstract).
Slingo, J., Spencer, H., Hoskins, B., Berrisford, P., Black, E., 2005. The meteorology of the western Indian ocean, and the influence of the east african Highlands. Phil. Trans. Math. Phys. Eng. Sci. 363 (1826), 25–42.
Smol, J.P., Stoermer, E.F., 2010. Applications and uses of diatoms: prologue. In: Smol, J. P., Stoermer, E.F. (Eds.), The Diatoms: Applications for the Environmental and Earth Sciences, second ed. Cambridge University Press, New York, pp. 3–7.
Socolar, J.B., Gilroy, J.J., Kunin, W.E., Edwards, D.P., 2016. How should beta-diversity inform biodiversity conservation? Trends Ecol. Evol. 31, 67–80. https://doi.org/10.1016/j.tree.2015.11.005.
Stager, J.C., Johnson, T.C., 2008. The Late Pleistocene desiccation of Lake Victoria and the origin of its endemic biota. Hydrobiologia 596, 5e16.
Stanley, D.J., Warne, A.G., 1993a. Nile Delta: recent geological evolution and human impact. Science 260, 628–634.
Stanley, D.J., Warne, A.G., 1993b. Sea level and initiation of Predynastic culture in the Nile delta. Nature 363, 435.
Stanley, D.J., Clemente, P.L., 2017. Increased land subsidence and Sea-Level rise are submerging Egypt's Nile Delta coastal margin. GSA Today 27 (5), 4–11. https://doi.org/10.1130/GSATG312A.1.
Stanley, D.J., Mcrea, J.E., Waldron, J.C., 1996. Nile Delta drill core and sample database for 1985-1994: Mediterranean Basin (MEDIBA) program. Smithson. Contrib. Mar. Sci. 37, 1–428.
Talling, J.F., 2009. Physical and chemical water characteristics. In: Dumont, H.J. (Ed.), The Nile: Origin, Environments, Limnology and Human Use. Monographiae Biologicae 89. Springer, Dordrecht, pp. 367–394.
ter Braak, C.J.F., Smilauer, P., 2002. Canoco for Windows Version 4.5. Biometrics-plant research international, Wageningen, Netherlands.
Tierney, J.E., de Menocal, P.B., 2013. Abrupt shifts in horn of Africa hydroclimate since the last glacial maximum. Science 342 (6160), 843–846.
Tierney, J.E., Russell, J.M., Huang, Y., Sinninghe Damsté, J.S., Hopmans, E.C., Cohen, A. S., 2008. Northern hemisphere controls on tropical southeast African climate during the past 60,000 years. Science 322 (5899), 252–255.
Tierney, J.E., Mayes, M.T., Meyer, N., Johnson, C., Swarzenski, P.W., Cohen, A.S., Russell, J.M., 2010. Late-twentieth-century warming in Lake Tanganyika unprecedented since AD 500. Nat. Geosci. 3, 422–425.
Tierney, J.E., Russell, J.M., Damst, Sinninghe, Huang, Y., Verschuren, D., 2011. Late quaternary behavior of the east african monsoon and the importance of the Congo Air boundary. Quat. Sci. Rev. 30, 798–807.
Tierney, J.E., Pausata, F.S.R., De Menocal, P.B., 2017. Rainfall regimes of the green Sahara. Sci. Adv. 3 (1), e1601503.
Uścinowicz, S., Zachowicz, J., Miotk-Szpiganowicz, G., Witkowski, A., 2007. Southern Baltic sea-level oscillations: new radiocarbon,pollen and diatom proof of the Puck Lagoon (Poland). Spec. Pap. Geol. Soc. Am. 426, 143–158.
Vadsaria, T., Ramstein, G., Dutay, J.C., Li, L., Ayache, M., Richon, C., 2019. Simulating the occurrence of the last sapropel event (S1): Mediterranean basin ocean dynamics simulations using Nd isotopic composition modeling. Paleoceanogr. Paleoclimatol. 34, 237–251.
van Dam, H., Mertens, A., Sinkeldam, J., 1994. A coded checklist and ecological indicator values of freshwater diatoms from The Netherlands. Net. J. Aquat. Ecol. 28, 117–133. https://doi.org/10.1007/BF02334251.
Van De Vijver, B., Van Kerckvoorde, A., Beyens, L., 2003. Freshwater and terrestrial moss diatom assemblages of the Cambridge Bay area, Victoria Island (Nunavut, Canada). Nova Hedwigia 225–243.
Vizy, E.K., Cook, K.H., 2003. Connections between the summer East African and Indian rainfall regimes. J. Geophys. Res. Atmos. 108 (D16).
Vos, P.C., De Wolf, H., 1993. Diatoms as a tool for reconstructing sedimentary environments in coastal wetlands; metodological aspects. Hydrobiologia 269, 285–296.
Wang, Y., Zhao, X.S., Salem, A., Shetaia, S.A., Zhang, F., Sun, C.P., Li, L.L., Liu, Y., Sun, Q.L., Chen, J., Li, M.T., Finlayson, B., Chen, Z., 2022. Deciphering hydroclimate fluctuations of Nile watershed from Holocene sediment of Manzala lagoon: bio-geochemical implications. Palaeogeogr. Palaeoclimatol. Palaeoecol. 601, 111141.
Williams, M.A., Williams, F.M., Duller, G.A., Munro, R.N., El Tom, O.A., Barrows, T.T., Macklin, M., Woodward, J., Talbot, M.R., Haberlah, D., Fluin, J., 2010. Late Quaternary floods and droughts in the Nile valley, Sudan: new evidence from optically stimulated luminescence and AMS radiocarbon dating. Quat. Sci. Rev. 29 (9–10), 1116–1137.
Winsborough, B.M., Shimada, I., Newsom, L.A., Jones, J.G., Segura, R.A., 2012. Paleoenvironmental catastrophies on the Peruvian coast revealed in lagoon sediment cores from Pachacamac. J. Archaeol. Sci. 39 (3), 602–614.
Wolman, M.G., Giegengack, R.R., 2007. The Nile River: geology, hydrology, hydraulic society. In: Gupta, A. (Ed.), Large Rivers pp.471–490.
Woodward, J.C., Macklin, M.G., Krom, M.D., Williams, M.A.J., 2007. The Nile: evolution, quaternary river environments and material fluxes. In: Gupta, A. (Ed.), Large Rivers: Geomorphology and Management. John Wiley & Sons, Chichester, pp. 261–292.
Zaki, A.S., King, G.E., Haghipour, N., Giegengack, R., Watkins, S.E., Gupta, S., Schuster, M., Khairy, H., Ahmed, S., El-Wakil, M., Eltayeb, S.A., 2021. Did increased flooding during the African Humid Period force migration of modern humans from the Nile Valley? Quat. Sci. Rev. 272, 107200.
Zalat, A.A., 2000. Distribution and paleoecological significance of fossil diatom assemblages from the Holocene sediments of Lake Manzala, Egypt. Diatom Res. 15 (1), 167–190.

Zalat, A.A., 2015. Holocene diatom assemblages and their palaeoenvironmental interpretations in Fayoum Depression, Western Desert, Egypt. Quat. Int. 369, 86–98.
Zalat, A.A., El-Sheekh, M.M., 1999. Diatom assemblages from two brackish Egyptian lakes. Egypt. J. Bot. 39 (1), 53–76.
Zalat, A.A., Vildary, S.S., 2007. Environmental change in Northern Egyptian Delta lakes during the late Holocene, based on diatom analysis. J. Paleolimnol. 37, 273e299.
Zhang, F., Hu, J.F., Li, X.X., Wang, Y.N., Salem, A., Sun, C.P., Zhao, X., Zhao, X.S., Jiang, F., Liu, Y., Shetaia, S.A., Chen, Z., 2022. Reconstruction of the Holocene hydro-ecological and environmental change of the Nile Delta: insights from organic geochemical records in MZ-1 sediment core. Mar. Geol. 443, 106684.
Zhao, X.S., Thomas, I., Salem, A., Alassal, S.E., Liu, Y., Sun, Q.L., Chen, J., Ma, F.W., Finlayson, B., Chen, Z., 2020. Holocene climate change and its influence on early agriculture in the Nile, Delta, Egypt. Palaeogeogr. Palaeoclimatol. Palaeoecol. 547, 109702.
Zong, Y., Kemp, A.C., Yu, F., Lloyd, J.M., Huang, G., Yim, W.W.S., 2010. Diatoms from the Pearl River estuary, China and their suitability as water salinity indicators for coastal environments. Mar. Micropaleontol. 75 (1–4), 38–49.